Excitation mechanism of atmospheric pressure waves from the 1980 Mount St. Helens eruption

AUTHOR(S):

Mikumo, Takeshi; Bolt, Bruce A.

CITATION:

Mikumo, Takeshi ...[et al]. Excitation mechanism of atmospheric pressure waves from the 1980 Mount St. Helens eruption. Geophysical Journal of the Royal Astronomical Society 1985, 81(2): 445-461

ISSUE DATE:

1985-05

URL:

http://hdl.handle.net/2433/193396

Geophys. J. R. astr. Soc. (1981) **65**, 129–153

A possible rupture process of slow earthquakes on a frictional fault

Takeshi Mikumo *Disaster Prevention Research Institute, Kyoto University, Uji, Kyoto 611, Japan*

Received 1980 May 29; in original form 1980 January 7

Summary. A possible mechanism for the occurrence of slow earthquakes is investigated by calculating numerical solutions for the dynamical rupture process on a quasi-three-dimensional fault with heterogeneous frictional strengths. Experimental friction laws for the dependence of sliding frictional stress on slip velocity, which are based on the cohesive properties of fault asperities, are taken into considerations.

It is found that the applied stress does not drop very rapidly with time and the rupture velocity remarkably decreases as the dependence on slip-velocity becomes smaller. These deceleration effects for the rupture propagation are greatly enhanced with increasing heterogeneities in the distribution of frictional strength and as the initial shear stress has lower levels with respect to the average strength. For these cases, the growth of rupture is extremely slow in a nucleus region with the dimension as large as 10 times the initial rupture length, and gains a terminal velocity dependent on the above factors. The displacement–time function becomes noticeably extended in these cases, and indicates a stick–slip-like phenomena in the extended time interval for a strongly heterogeneous fault.

It seems that these results could explain the characteristic features of slow earthquakes.

1 Introduction

Much evidence has recently been provided by various observations that there are actually a number of 'slow earthquakes' with unusually long duration of the rupture process at the source. It has been inferred from observations of long-period seismic waves that several tsunami earthquakes which occurred near deep-sea trenches, as well as a series of multiple events along a transform fault, had long time constants up to several minutes (Kanamori 1972; Fukao & Furumoto 1975; Geller & Shimazaki 1978; Pfluke 1978; Fukao 1979; Kanamori & Stewart 1979). Similar observations have been reported for deep-focus Columbian earthquakes (Dziewonski & Gilbert 1974) and an anomalously large intermediate-depth earthquake east of Hokkaido, Japan (Kasahara & Sasantani 1979; Sudo, Sasatani & Kasahara 1979). Besides these observations, it appears that several moderate-size earthquakes

around the Japan Islands may be regarded as 'low-frequency earthquakes' (Utsu 1979, private communication).

Much slower crustal deformations with rise times 10–20 min or longer have also been suggested from the records of strainmeters, tiltmeters, tide-gauges etc., for a precursory slip of the 1960 Chilean earthquake (Kanamori & Cipar 1974), coseismic fault movements during the 1946 Nankaido earthquake (Ando 1975), coseismic and in some cases preseismic movements at the time of a few crustal earthquakes in Japan (Sacks *et al.* 1978) and in China (Nagamune 1977). On the other hand, there have been several observations of creep events taking place repeatedly along the San Andreas fault in central California (e.g. Tocher 1960; Nason 1971; Bufe, Bakun & Tocher 1973; King, Nason & Tocher 1973), which have the time duration of 30 min to 3–4 day, and of large strain transients in the central Aleutians (Major & Tocher 1971) and in Nevada (Smith & Kind 1972). These 'silent' events may be interpreted as the results of aseismic fault slip at depth. There is also some evidence that anomalous crustal deformations, several hours to several years preceding great earthquakes, might be attributed to precursory fault movements (e.g. Fujii 1978).

The unusual slow rise times experienced in the above earthquakes and creep-like deformations suggest very low rupture velocities propagating over the fault plane, and hence may be associated closely with the properties of materials on the fault zone such as of fault gouges, asperities or barriers and so on. Detailed studies on the time history of these slow earthquakes seem very important for a better understanding of the constitutive laws for the fault material, the process of stress concentration and of the triggering mechanism for normal earthquakes.

The purpose of the present paper is to provide a possible explanation to the problem under what physical conditions a slow rupture process could arise. For slow propagation of creep events, and for the migration of seismic activity, a few theoretical models have already been proposed; the flow of edge dislocations along a transform fault with a non-elastic fault zone (Savage 1971), which is based on the kinematic wave theory, propagating edge and screw dislocations along a zone of plastic fault gouge with some constitutive equations (Nason & Weertman 1973), and uniform propagation of a viscous crack in fault gouge under a quasi-static stress field (Ida 1974). It has also been suggested that the slow process of tsunami earthquakes may be due to the viscoelastic properties of a partially melted or fractured fault zone (Kanamori 1972; Fukao & Furumoto 1975). On the other hand, Weertman (1969) suggested that slow creep-like slippage will occur over finite distances when a slowly increasing external shear stress plus the internal stress caused by stationary dislocations first equals the lowest frictional strength if the strength is non-uniform. A recent work of Yamashita (1980) introduces inhomogeneous initial stress, sliding frictional stress and specific fracture energy into two-dimensional longitudinal shear cracks to account for the causes of slow earthquakes and multiple events.

In the present paper, we will focus our attention on the cohesive properties of fault zone material, and particularly on the role of asperities on the fault surface, which should have some friction laws like constitutive equations. We are mainly concerned here with the dependence of sliding frictional stress on slip velocity on the fault, which has been estimated from laboratory experiments on friction for rock materials. Our approach here is to provide numerical solutions to the dynamical process on a frictional fault with these friction laws, to clarify how slow earthquakes could take place.

2 Fault model

The model we are considering here is essentially based on the quasi-three-dimensional fault as introduced in a previous paper (Mikumo & Miyatake 1978, henceforth Paper I), in which

static and sliding frictional stresses are non-uniformly distributed and being subjected to a finite shear stress. These non-uniformities have been introduced to represent heterogeneous properties of fault material which has asperities or high strength barriers on the fault surface. This model provided satisfactory explanations to the initiation, spreading and stopping of rupture, stick–slip instability, radiation of high-frequency seismic waves, and non-uniform fault displacements, as well as to the occurrence of a main shock, multiple events, after-shocks on a single fault, and its statistics including magnitude frequency relationship (Mikumo & Miyatake 1979, henceforth Paper II), while it did not account for aseismic fault slip. In this model, sliding frictional stress was assumed to be a function of position on the fault, but independent of time, slip displacement and slip velocity. If we introduce, however, non-elastic fault material such as a viscous layer or viscoelastic zone into the fault, the stress should be dependent on slip displacement and/or velocity. Dynamical solutions for these cases can be obtained in a similar way to that in Paper I, but it seems rather difficult to estimate the relevant non-elastic parameters from laboratory experiments.

The approach taken here is based on the characteristic friction laws on rock materials. It has been suggested (Weertman 1969) on the basis of friction experiments on metals (Bowden & Tabor 1964) that the frictional stress required to produce slippage across the fault interface decreases with increasing slip velocity. The velocity dependence of sliding friction is also found in friction experiments on silicate rocks (Scholz & Engelder 1976; Dieterich 1978). These friction characteristics are explained (Scholz & Engelder 1976) by the role of indentation and ploughing of asperities on the sliding surface; the process that yields stick–slip instability in the frictional sliding is attributed to creep of indentation asperities on the surface, resulting from stress corrosion cracking or hydrolytic weakening, which leads to the increase in real area of contact with time; this in turn yields increases in friction with increasing time of stationary contact or decreasing sliding velocity (Scholz & Engelder 1976). This feature is consistent with a slightly modified form of the Bowden & Tabor (1964) adhesion theory. From the laboratory data shown in Fig. 1, the following empirical forms have been given to relate the coefficient of sliding friction μ_d to slip velocity V,

$$\mu_d = (1 - \beta \log V)\bar{\mu}_d \qquad \text{(Scholz \& Engelder 1976)} \qquad (1)$$

$$\mu_d = \mu_0 + \alpha \log (bD_c/V + 1) \qquad \text{(Dieterich 1978)} \qquad (2)$$

analogous to the time dependence of static friction, although a more complex form has been proposed later (Dieterich 1979) to explain details of different experiments. μ_0 and $\bar{\mu}_d$ are the dynamic friction coefficients at a specific sliding velocity and at the average velocity, respectively, and α, β and b are numerical constants. For several experiments, these constants have been estimated as; $\beta = 0.07 \pm 0.02$, $\bar{\mu}_d = 0.49 \pm 0.03$, $\alpha \cong 0.02$ and $b = 1.0$–2.0. D_c is defined as the critical dimension of the contact of asperities and hence D_c/V is regarded as an average life time of a population of contacts (Dieterich 1978). These two forms are essentially similar except for higher slip velocities.

The experimental results of Scholz & Engelder (1976) shown in Fig. 1 indicate weak displacement dependence of sliding friction for smaller displacements in the case of constant velocity. Since the sliding friction should level down from static friction, we tentatively use a slightly modified form,

$$\mu_d = \mu_s - \beta \log V + k\beta \log D \qquad (3)$$

introducing slip displacement D instead of D_c, where k estimated from the laboratory data is of the order of 0.2–0.4. The sliding frictional stress σ_d in this case may be written, by multiplying a normal stress σ_n to equation (3), as,

$$\sigma_d = \sigma_s + B(k \log D - \log V) \qquad (4)$$

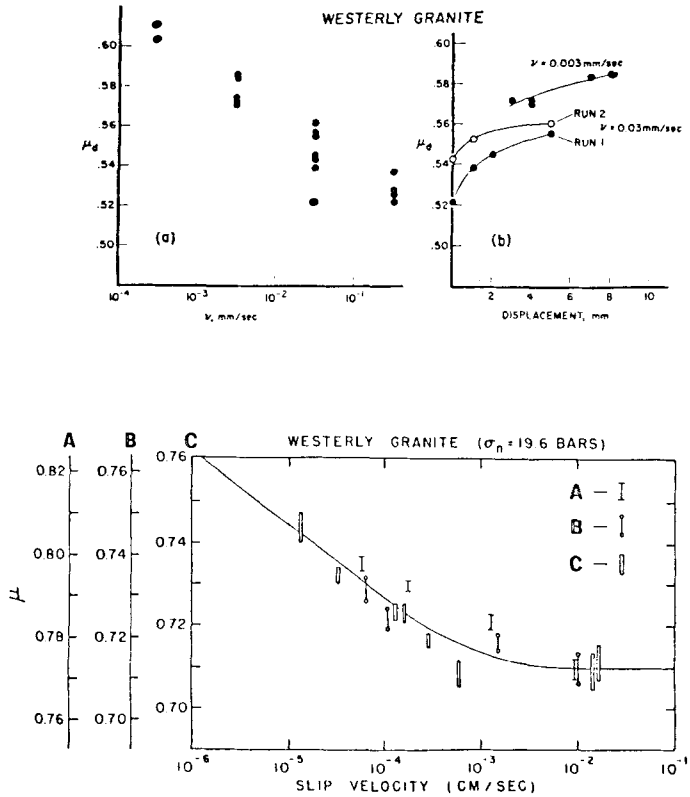

Figure 1. Laboratory friction data for Westerly granite, indicating the dependence of sliding friction on slip velocity and displacement. Upper: (a) sliding friction versus slip velocity, (b) sliding friction versus slip displacement after Scholz & Engelder (1976). Lower: sliding friction versus slip velocity after Dieterich (1978).

where $\sigma_d = \mu_d \sigma_n$, $\sigma_s = \mu_s \sigma_n$ and $B = \beta \sigma_n$. The variation of σ_d with time is,

$$\frac{d\sigma_d}{dt} = B\left(\frac{kV}{D} - \frac{1}{V}\frac{dV}{dt}\right) \tag{5}$$

and its incremental increase can be calculated by,

$$\sigma_d(t + \Delta t) = \sigma_d(t) + f(D, V)\Delta t \tag{6}$$

where $f(D, V)$ simply replaces the right side of equation (5). Fig. 2 shows a schematic representation of the time variations of σ_d for an assumed quadratic functional form of displacement at the initial stage, which gives the B-dependence for $k = 0$ and the k-dependence for a fixed B-value. This indicates, as expected from equation (5), that for larger B-values the sliding frictional stress drops very rapidly to its lowest value $\sigma_{d\cdot m}$ as soon as slip motion begins, corresponding to normal brittle fractures. For smaller B-values, however, the stress decreases slowly with time and takes time to reach the lowest value. In a slip weakening model (e.g. Andrews 1976), the initial stress is also assumed to drop gradually as slip displacement increases. It is shown, however, that the displacement dependence indicated by variations of k give smaller effects to the case of decreasing B-values. For this

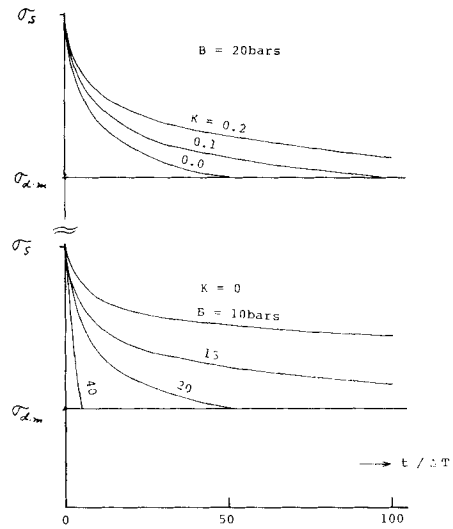

Figure 2. Schematic representation of the time variations of sliding frictional stress for an assumed quadratic increasing displacement at the initial stage. Upper: dependence of k for a constant B-value. Lower: dependence of B for $k = 0$.

reason, we are dealing only with the velocity dependence in the subsequent numerical solutions. σ_d also varies depending on the location of the fault if static frictional strength is non-uniformly distributed.

Now we introduce the above condition into the previous fault model in Paper I. The fracture criterion used here is a finite-stress criterion as in the foregoing model; once the initial shear stress exceeds the static frictional strength at each point on the fault, slip motion begins. In this case, the slip motion is resisted by the sliding frictional stress

Table 1. Parameters specifying frictional fault models in this study.

Case	σ_s			σ_d	B	σ_0
	min	avr (bar)	max	min (bar)	(bar)	(bar)
F		202		120		
		210		120		
		230		120	4, 6, 10, 20, 50, 100	200
		250		120		
		300		120		
A	200	319	578	100	6	208.6
					8	207
					10	205
					15, 20, 50, 100	204
B	200	282	641	120	6	208
					8	207
					10	206
					15	205
					20, 50, 100	204
C	200	260	320	120	8, 10, 20, 50, 100	204

Remarks: σ_s static frictional strength – min: minimum, avr: average, max: maximum. σ_d sliding frictional stress – min: minimum. σ_0 initial shear stress.

dependent on slip velocity V, which is given by equation (4) with $k = 0$. The external shear stress is assumed to increase very slowly (by about 4 bar yr^{-1}) due to the increase in tectonic loading resulting from relative plate movements with a velocity of 10 cm yr^{-1} (Paper II). This increase, however, has little effect on the rupture propagation within the time interval now in consideration. Under these conditions, numerical solutions are calculated for dynamical rupture propagation in various possible cases. The parameters specifying the fault model and other constants are taken as almost the same as in Paper I, except that $\Delta z = 8$ km to give larger displacements. The adopted static and lowest sliding frictional stresses and the initial stress are tabulated in Table 1.

3 Numerical solutions for slow rupture process

In this section, several representative results of numerical calculations are presented, which include the time–distance relation and the pattern of rupture propagation, and the displacement time function, all of which indicate the natures of slow earthquakes.

3.1 CASE OF HOMOGENEOUS STATIC FRICTIONAL STRENGTHS

We have worked out 30 cases. In these cases, the static frictional strength is assumed to be constant over the fault plane except at the starting point of rupture. The assumed strengths are 202, 210, 230, 250 and 300 bar, and the lowest sliding frictional stress is taken as 120 bar. The initial shear stress is also assumed to be homogeneous, being 200 bar or slightly larger. The B-value indicating the velocity dependence of the sliding frictional stress is taken here as ranging from 4 to 100 bar. When σ_0 is close to σ_s and also B is large, the case simply reduces to that treated in Paper I.

In the normal rupture process, the rupture front propagates with an elliptic shape with a nearly P-wave velocity in the direction parallel to the applied shear stress, and with a nearly S-wave velocity in the direction perpendicular to it, as shown in Paper I. For the fault dimension of 40×40 km, the rupture initiating from the centre of the fault reaches the prescribed fault edges in 3.7 and 6.3 s in the two directions, respectively. To compare with this normal case, an example of the rupture pattern in the present calculations is given in Fig. 3. Numerals on the rupture fronts indicate the propagation time elapsed after the rupture initiation. We see that in Case F with $\sigma_s = 250$ bar it takes a much longer time for the rupture to cover the entire fault surface as compared with the normal process. Also noticeable here are the effects of decreasing B-values, which indicate the increase in the rupture propagation time from about 12 to 60 s at the left end of the fault as B decreases from 50 to 4 bar. The effects will be discussed later in more detail.

Fig. 4(a)–(d) gives the time taken for rupture to propagate to different distances, for four different values of σ_s with a parameter of B. The x- and y-axes here are taken parallel and perpendicular to the applied shear stress and measured from the starting point of rupture. From these figures, the following obvious features are immediately noticed. For fixed σ_s and B-values the rupture propagation takes more time in the y-direction than in the x-direction, indicating an elliptical mode of propagation as expected from the previous results. It has been pointed out, however, that this is not always the case in the normal rupture process on a more complete three-dimensional fault (Miyatake 1980); if the static frictional strength is considerably larger than the applied stress, the rupture tends to show a circular propagation (Miyatake 1980) with decreased velocities in the x-direction. For this reason, only the curves in the y-direction is presented for $\sigma_s = 300$ bar.

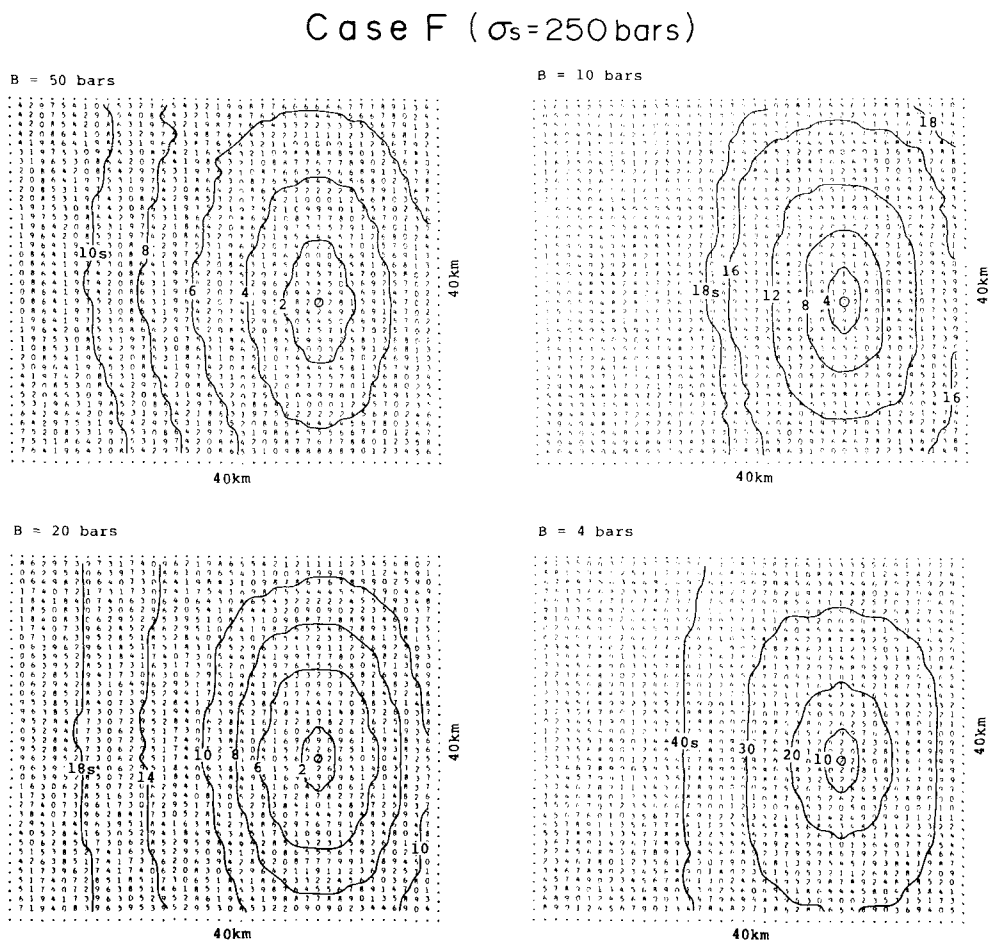

Figure 3. Rupture patterns in Case F with σ_s = 250 bar, for B-values ranging from 50 to 4 bar.

It is also noticed from a comparison between Fig. 4(a)–(d) that for a fixed B-value the rupture propagates more slowly as the static frictional strength σ_s has higher levels with respect to the applied stress σ_0. When σ_s is elevated from 210 to 300 bar, the propagation time of rupture to reach a position at y = 20 km increases from 5.6 to 18.6 s for B = 50 bar and from 15.6 to 97.5 s for B = 4 bar. This type of variation in the rupture velocity has been suggested analytically in two-dimensional shear cracks (e.g. Burridge 1973; Andrews 1976) and numerically in a three-dimensional fault (Miyatake 1980), although these studies do not involve the effect of velocity dependence of sliding frictional stress. Although the above decrease in the rupture velocity is not a new finding here, the difference in the stress level could be one of possible sources for slow earthquakes, and the effect would be enhanced if combined with other sources.

The most remarkable feature to be noted here is that for a fixed value of σ_s the propagation time of rupture rapidly increases with decreasing B-values. The rates increase by a factor of 2.8, 4.8 and 5.3 respectively in the case of σ_s = 210, 250 and 300 bar when B decreases from 50 to 4 bar. This clearly indicates that small B-values greatly decelerate the rupture propagation. This effect results from the assumed cohesive properties of fault material due to ploughing asperities on the fault surface. From the laboratory data for a

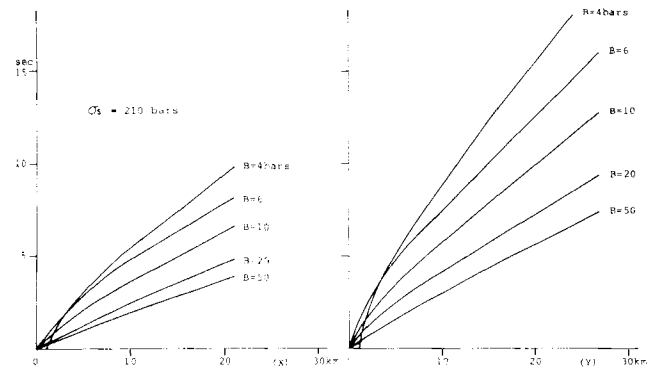

(a)

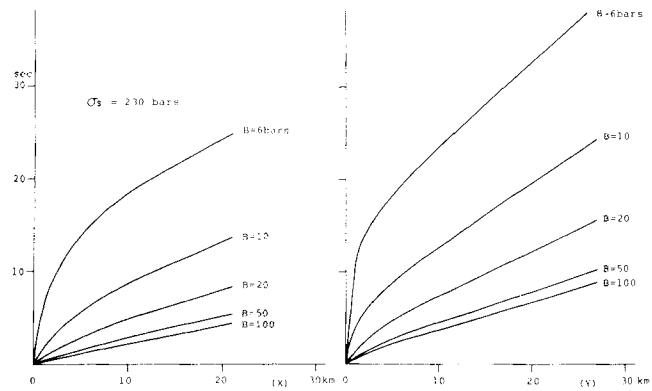

(b)

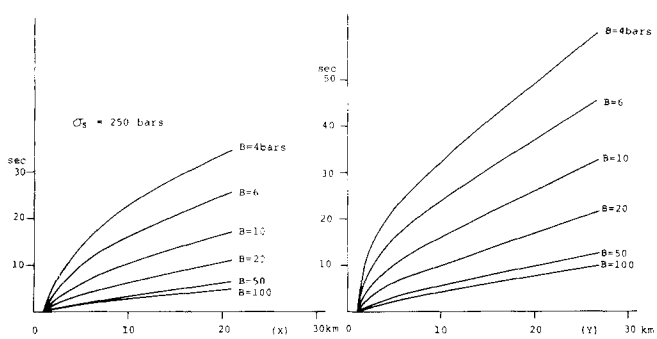

(c)

Figure 4. The time taken for rupture to propagate over the fault plane with various B-values (ordinate) against given distances (abscissa). Left: rupture propagation time in the x-direction parallel to the applied shear stress. Right: rupture propagation time in the y-direction perpendicular to the applied shear stress. (a) For σ_s = 210 bar, (b) for σ_s = 230 bar, (c) for σ_s = 250 bar, (d) for σ_s = 300 bar.

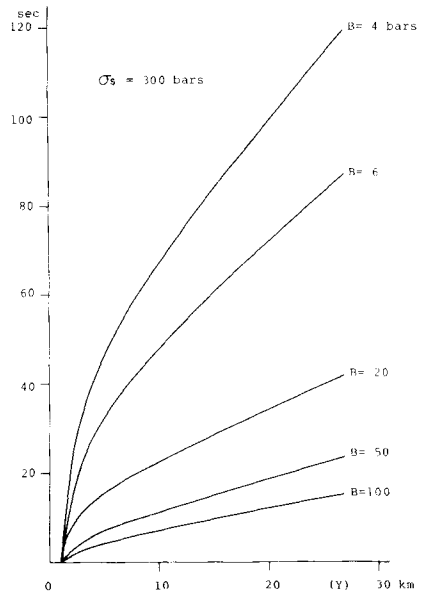

Figure 4 (d)

limited number of rocks (Scholz & Engelder 1976), the B-value in this case may be of the order of 5–20 bar for $\sigma_s = 200$–300 bar, which is small enough to cause slow rupture propagations.

Another important feature is the transient nature of rupture velocities. As is clear from Fig. 4(a)–(d), the rupture moves very slowly at the initial stage, then gradually increases its propagation velocities up to a distance of about 6–10 km, and finally gains a terminal velocity, for all cases of σ_s and B-values. It has been stated (Andrews 1976) that a plane-strain shear crack with a slip-weakening law shows slow initial growth of rupture up to a distance comparable to the doubled initial crack length, with its terminal velocity approaching the Rayleigh velocity. To compare with this, the initial and terminal velocities in the y-direction perpendicular to the applied stress are explicitly shown in Fig. 5, as a

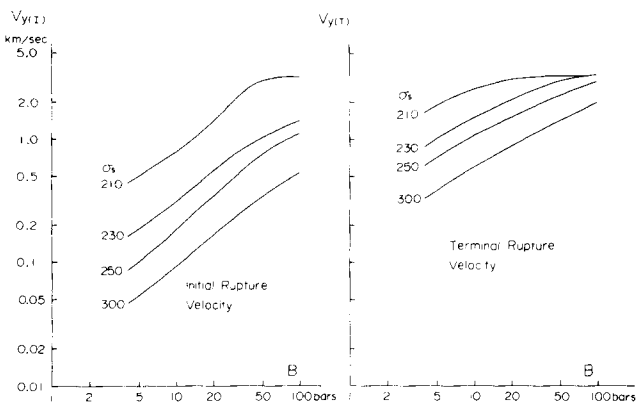

Figure 5. Initial rupture velocity (left) and terminal rupture velocity (right) in the y-direction, against B-values with a parameter of σ_s.

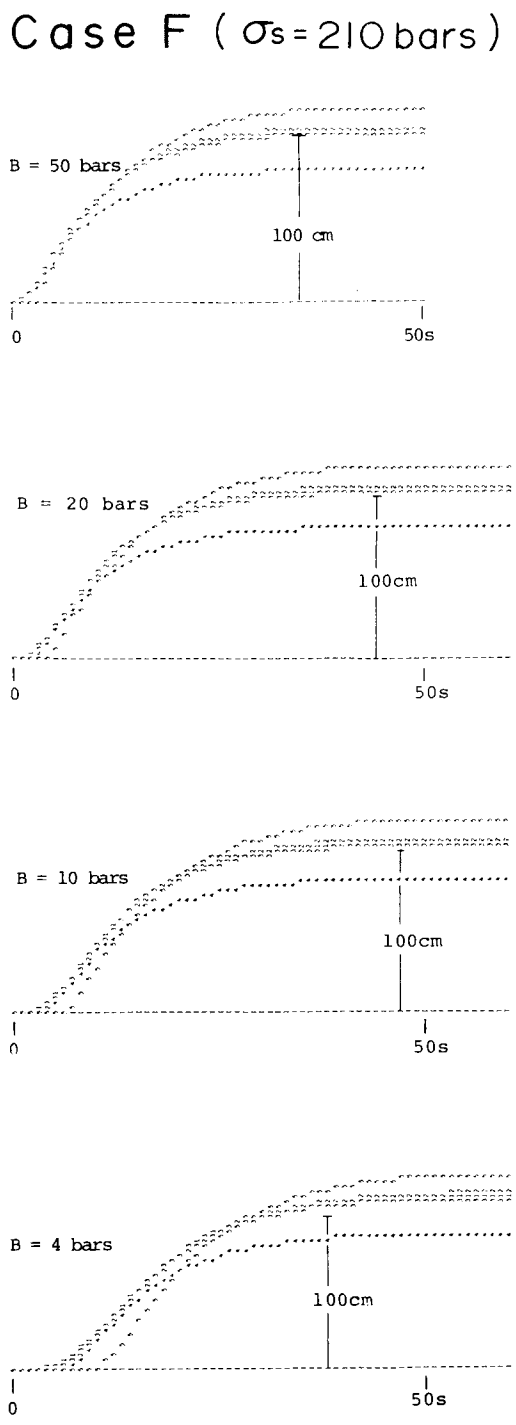

(a)

Figure 6. Displacement–time functions at several selected points on the fault, for four different B-values. Ordinate indicates the displacement and abscissa indicates time in seconds. Different symbols used indicate the location. 1: x = 23 km, y = 29 km, 2: x = 25 km, y = 27 km, 3: x = 20 km, y = 30 km, 4: x = 30 km, y = 30 km, 5: x = 20 km, y = 20 km. (a) Case F with σ_s = 210 bar, (b) Case F with σ_s = 250 bar, (c) Case F with σ_s = 300 bar.

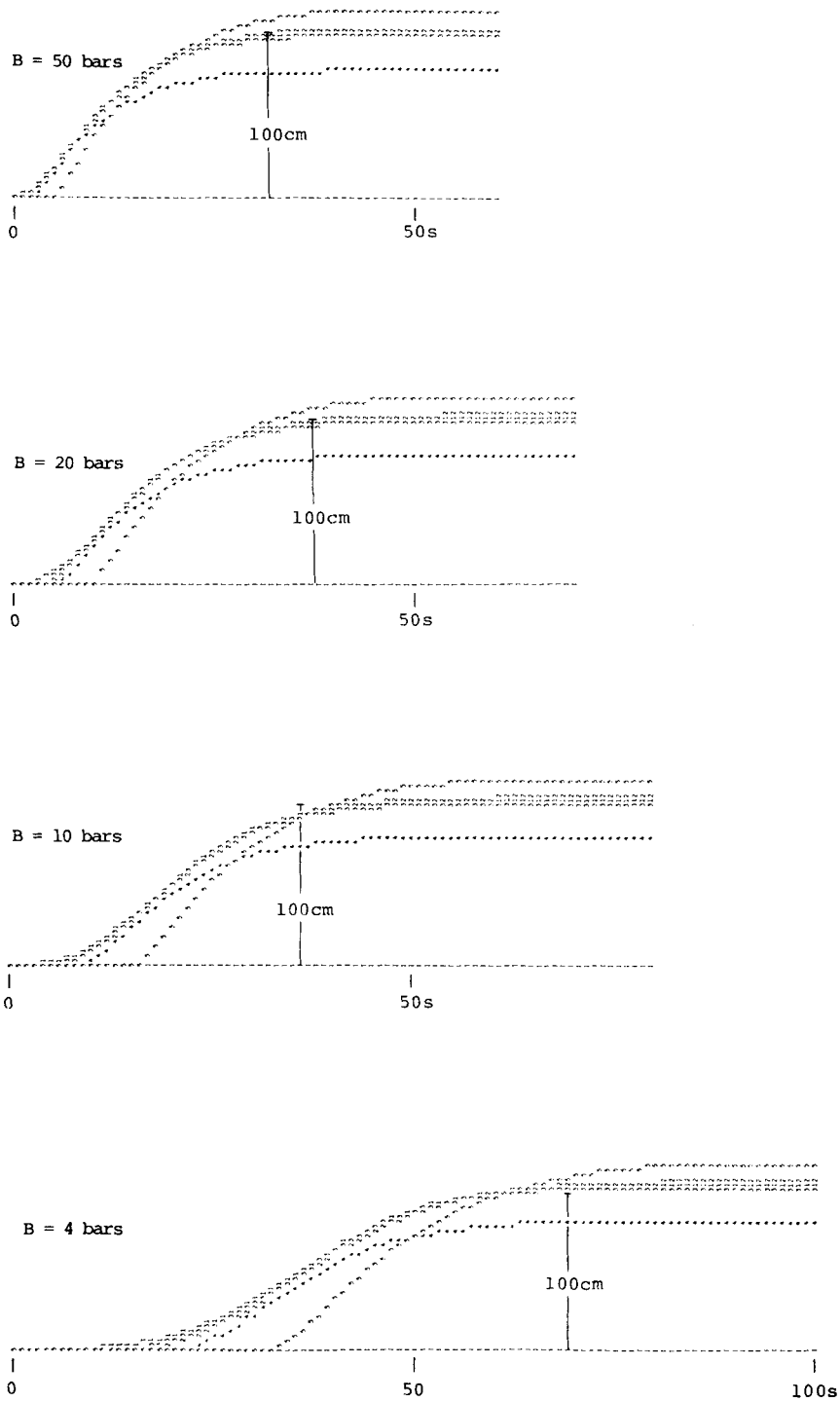

Figure 6 (b)

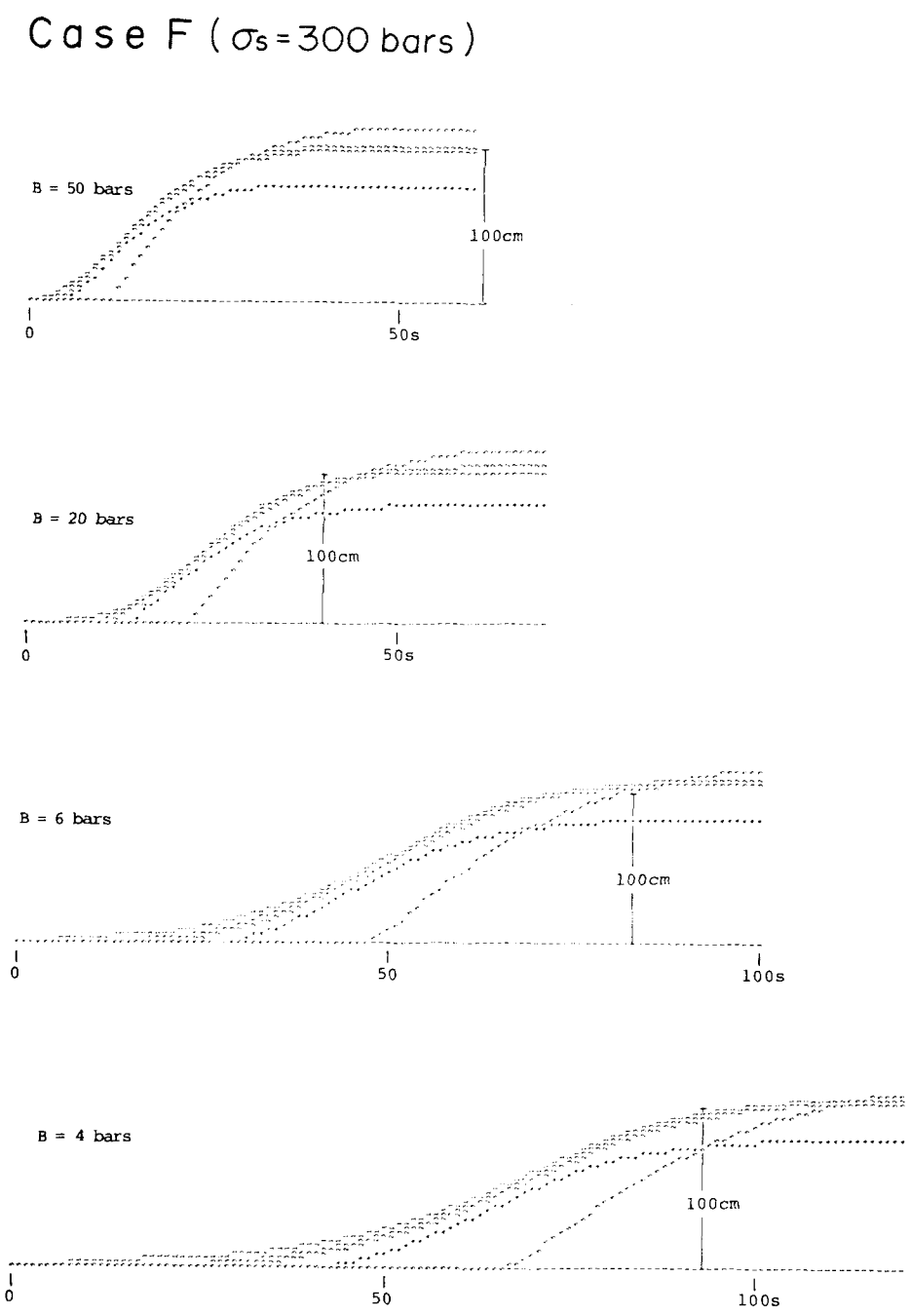

Figure 6 (c)

function of the B-values with a parameter of σ_s. It is obvious that both of the velocities are much reduced for smaller B and larger σ_s. The terminal velocity for large B-values approaches the S-wave velocity. The initial velocity in the present calculations could go down to an extremely low value of 0.05 km s^{-1} or less. This suggests that the rupture grows up very slowly up to a finite dimension, the length of which is of the order of 10 km. The dimension

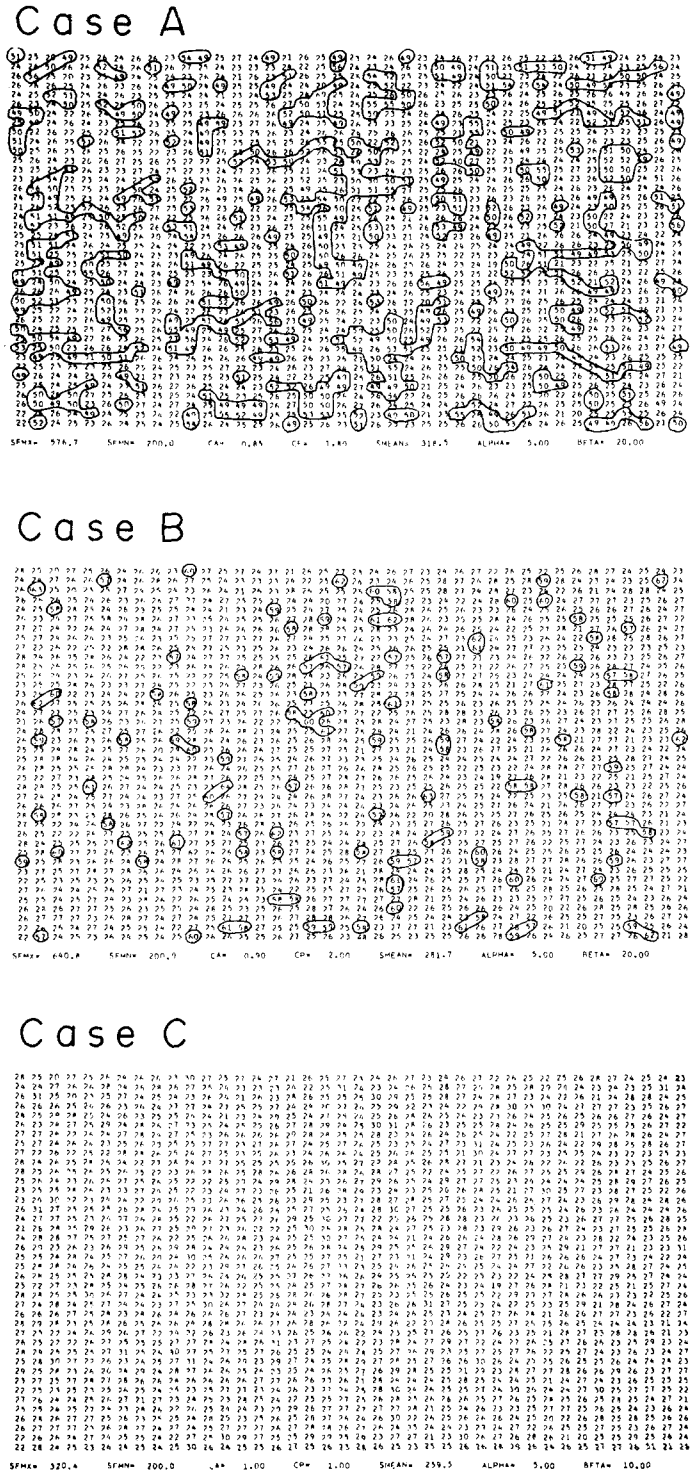

Figure 7. Three different types of heterogeneous distribution of static frictional strength. Case A: most heterogeneous, including high strength exceeding 500 bar, Case B: moderately heterogeneous, with smaller inclusions with higher strength, Case C: weakly heterogeneous.

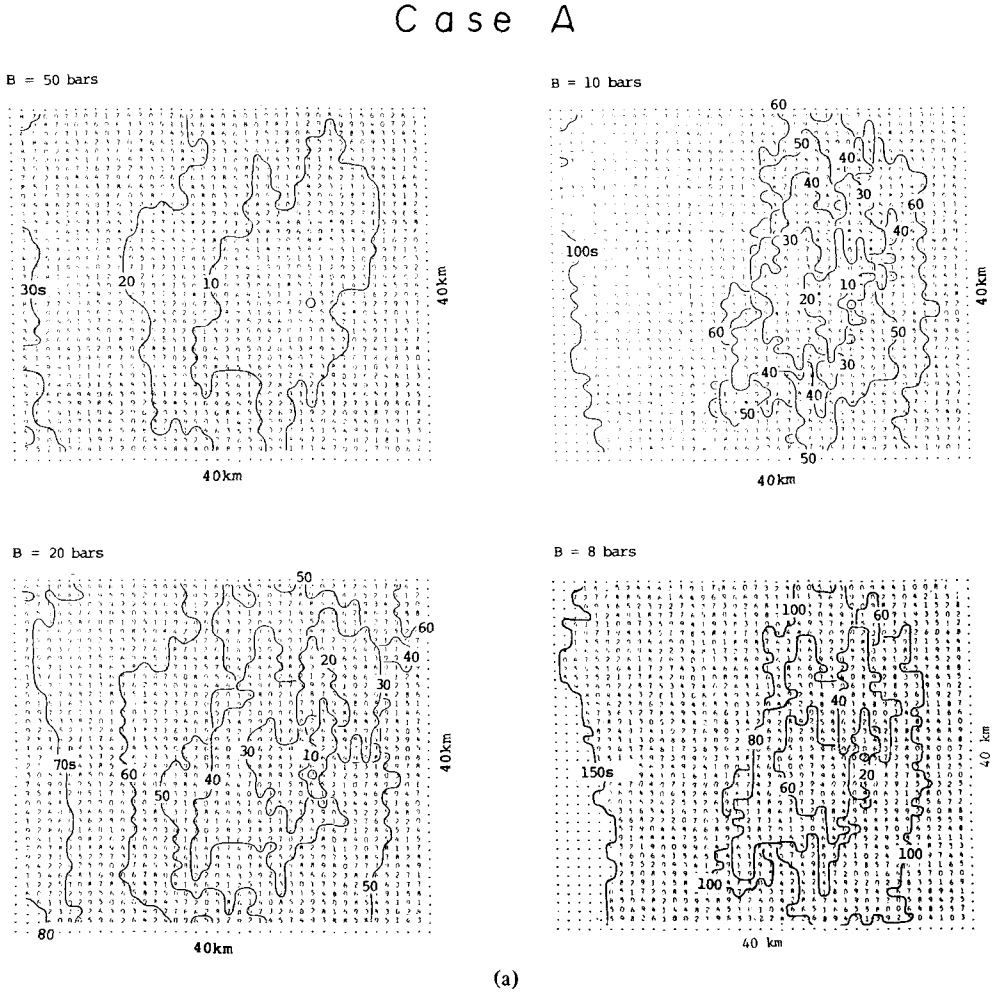

(a)

Figure 8. Patterns of rupture propagation for different B-values. (a) Case A, (b) Case B, (c) Case C.

in this case does not seem to be dependent on the stress level, but might be regarded as the nucleus of a slow earthquake, where strain energies are accumulated for further accelerating ruptures. It is not clear, at this moment, what conditions specify the nucleus area.

Fig. 6(a)–(c) illustrate the displacement time function at several selected points on the fault, in Case F for $\sigma_s = 210$, 250 and 300 bar with various values of the parameter B. These points are the starting point of rupture ($x = 23$ km, $y = 29$ km), three points ($x = 25$ km, $y = 27$ km; $x = 20$ km, $y = 30$ km; $x = 30$ km, $y = 30$ km) close to the starting point and the centre of the fault ($x = 20$ km, $y = 20$ km), where the x- and y-coordinates are measured downwards and to the right from the left top corner of Fig. 3. In the case of $\sigma_s = 210$ bar, the time history does not appear very different for four different B-values. If σ_s is elevated to 250 and 300 bar, it is clearly noticed that the time function becomes remarkably elongated with decreasing B-values. The rise time for $\sigma_s = 300$ bar increases from about 35 to 100 s as B decreases from 50 to 4 bar. The longest rise times shown here for $B = 4$ bar are approximately 40, 65 and 100 s for $\sigma_s = 210$, 250 and 300 bar, respectively. It has thus been demonstrated that slow rise times result from slow rupture propagation on the fault surface. A delayed onset of the time function included in these figures corresponds to the

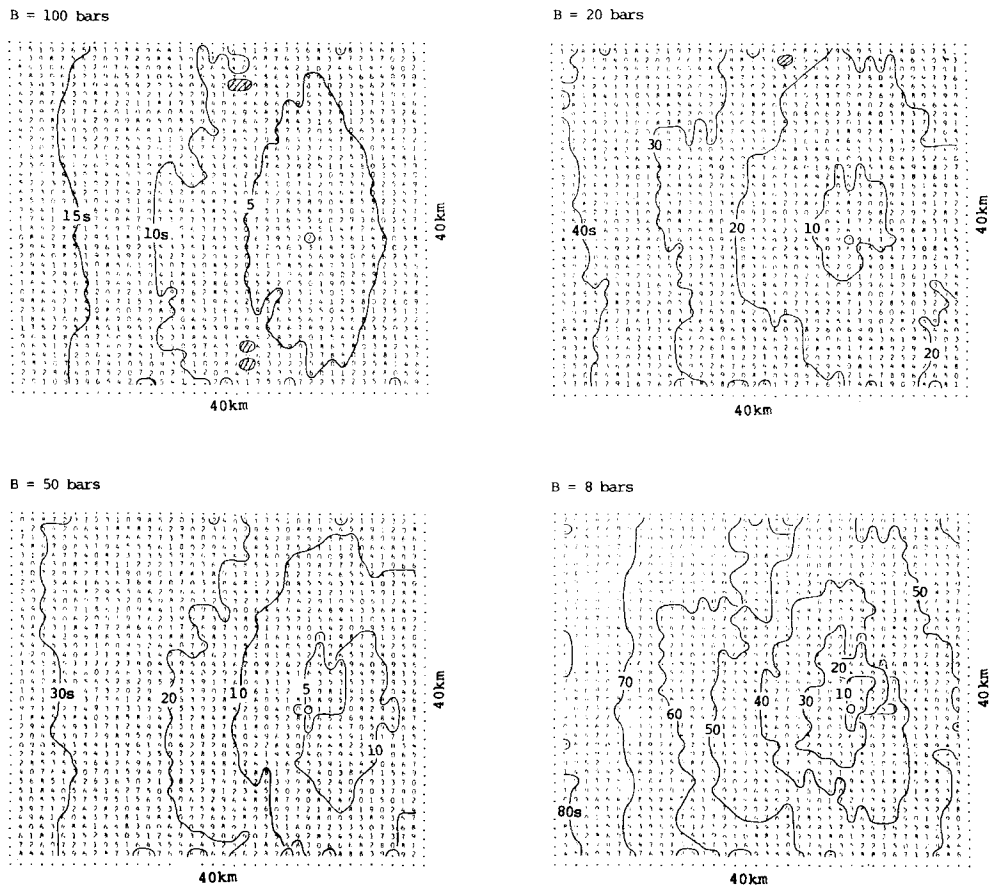

Figure 8 (b)

delayed arrival of the rupture to the centre of the fault (x = 20 km, y = 20 km). It should be remarked that the rise time at this point appears considerably shorter than that at the rupture initiating point unlike in the normal rupture process.

3.2 EFFECT OF HETEREOGENEOUS DISTRIBUTION OF STATIC AND SLIDING FRICTIONAL STRESSES

We have made a number of calculations for the various cases given in Table 1, in order to examine the effects of spatially heterogeneous distribution of static and sliding frictional stresses. Three different distributions are shown in Fig. 7, which are similar to those tested in Papers I and II (Mikumo & Miyatake 1978, 1979). Case A includes a number of high strengths exceeding 500 bar within the encircled portions, Case B has smaller inclusions with higher strengths, and Case C has a weakly heterogeneous distribution with a standard deviation of 25 bar. The average strength in these cases is 319, 282 and 260 bar, respectively. The sliding frictional stress in these cases is also non-uniformly distributed as indicated by equation (4), and their minimum value is taken as 100 bar in Case A and 120 bar in Cases B and C. The initial stress and B-values are taken as the same in the foregoing section.

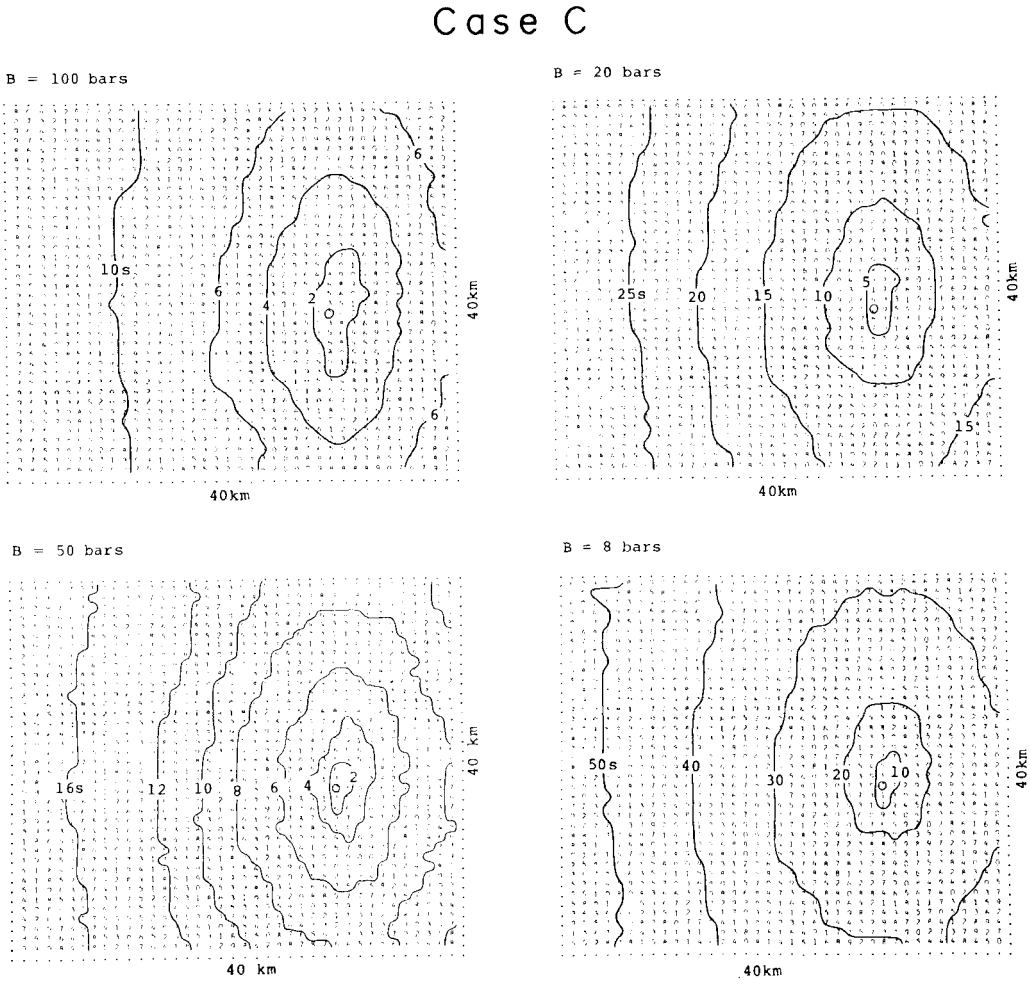

Figure 8 (c)

Fig. 8(a), (b) and (c) illustrate the patterns of rupture propagation in Cases A, B and C, respectively, for four different B-values. In Case C with the average strength of 260 bar, the rupture patterns are not very different from those in Case F with $\sigma_s = 250$ bar shown in Fig. 3. A close comparison between the two cases for $B = 50$ and 20 bar shows, however, that it requires a somewhat longer time in Case C than in Case F for the rupture to reach the left edge of the fault. For more heterogeneous cases, Cases A and B, the shape of the rupture fronts becomes strikingly complicated and its propagation velocity remarkably decreases, as high strength inclusion increases and as the B-value decreases. The rupture velocities in these two cases are given in Fig. 9, analogous to Fig. 5, where their possible ranges are shown by shaded zones and $V_{x(I)}$, $V_{y(I)}$ and $V_{y(T)}$ denote the average initial velocities in the x- and y-directions over a distance of 10 km and the terminal velocity in the y-direction, respectively. The decreases in the rupture velocity in these cases are again remarkable. In order to see more explicitly the effect of heterogeneities on the rupture velocity, Cases A and F with $\sigma_s = 300$ bar, which have nearly the same level of the average strength, are compared in Fig. 10 for $B = 6$ bar. The most obvious effects found in Case A, as compared with the pattern in Case F, are the irregularly deformed rupture fronts and much longer

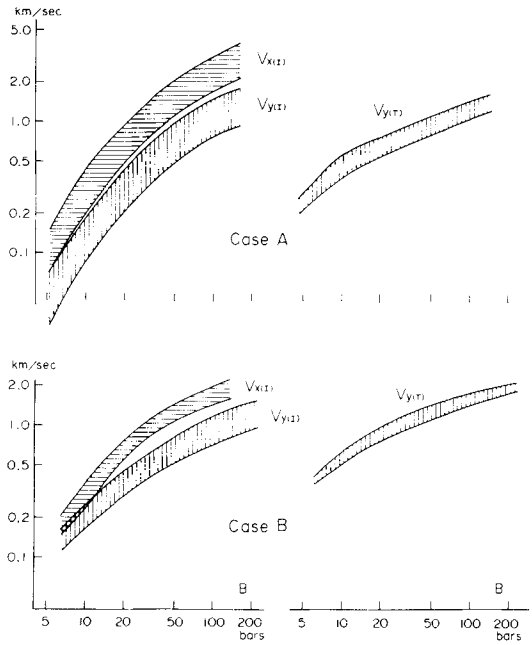

Figure 9. Rupture velocities against B-values as a parameter of σ_s. $V_{x(I)}$: initial rupture velocity in the x-direction, $V_{y(I)}$: initial rupture velocity in the y-direction, $V_{y(T)}$: terminal rupture velocity in the y-direction.

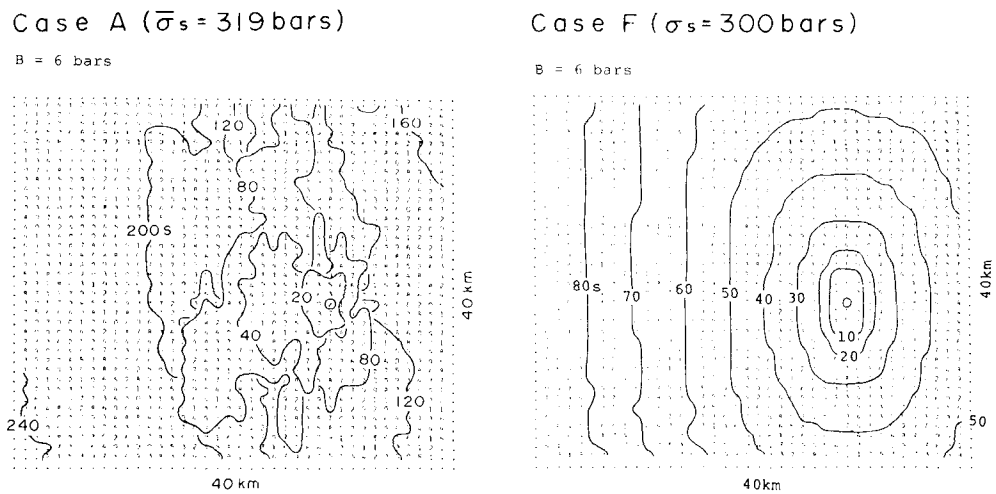

Figure 10. Rupture patterns in a most heterogeneous case Case A with $\bar{\sigma}_s$ = 319 bar and B = 6 bar, in comparison with those in Case F with σ_s = 300 bar and B = 6 bar.

propagation time of about 240 s to reach the left-bottom of the fault. It is thus demonstrated that strongly heterogeneous distribution of static and sliding frictional stresses also gives a dominant deceleration effect for rupture propagation. It can also be recognized in Case A that there is a nucleus zone where the initial rupture grows up in extremely slow speeds, although the initial velocity and the finiteness of the zone cannot be estimated correctly because of their appreciable difference in different directions.

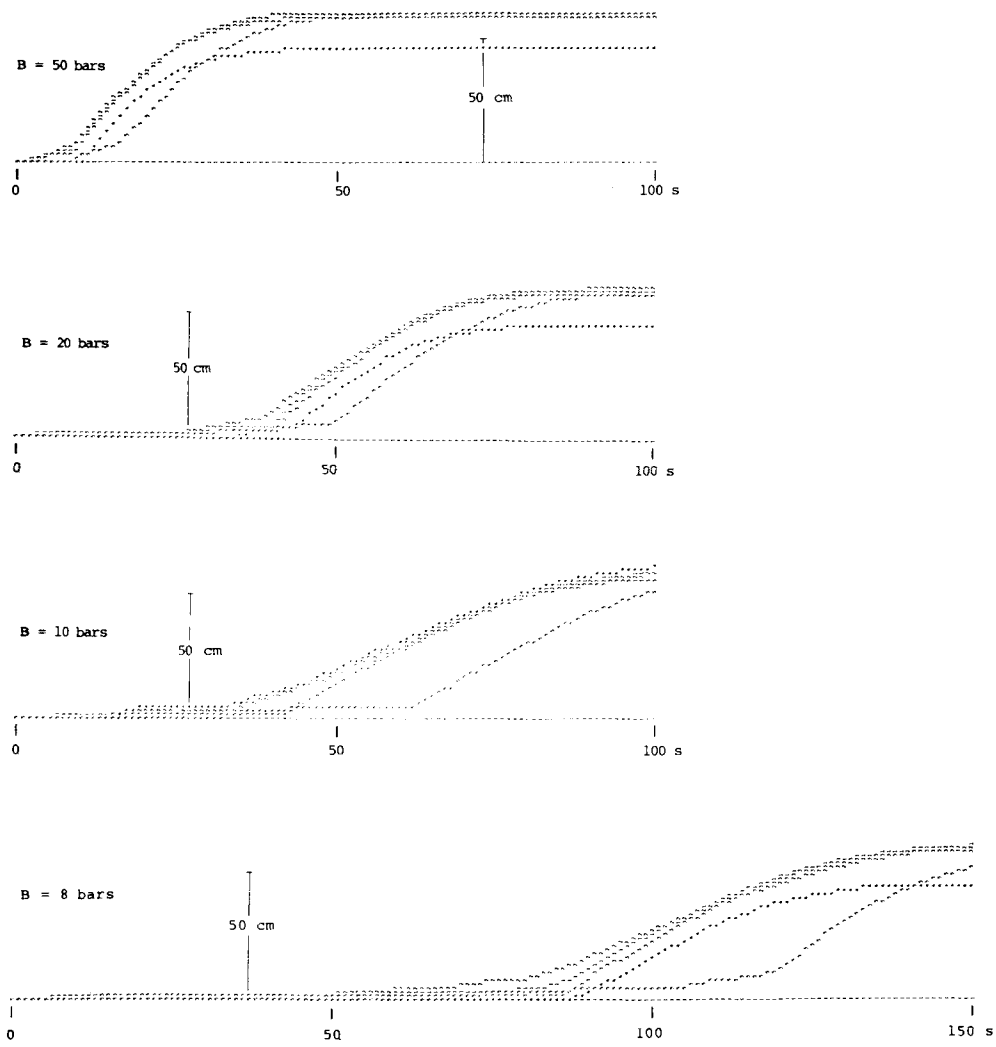

(a)

Figure 11. Displacement–time functions in three different types of heterogeneous fault, for different B-values. Different symbols indicate the function at the location given in Fig. 6. (a) Case A, (b) Case B, (c) Case C.

The displacement–time function in Cases A, B and C are shown in Fig. 11(a), (b) and (c), where the location of the selected points are the same as in Case F. It is found that elongations in the total time duration and gradual decreases in its initial slope with decreasing B-values are extremely noticeable. The rise times of the function in the three cases are also depicted in Fig. 12, which clearly shows a rapid increase for smaller B-values indicating the steepest rate for Case A. If we compare Case A with Case F for $\sigma_s = 300$ bar, and Case C with Case F for $\sigma_s = 250$ bar, it is again noticed that the effects of heterogeneities appears remarkable in the displacement–time function.

Case B

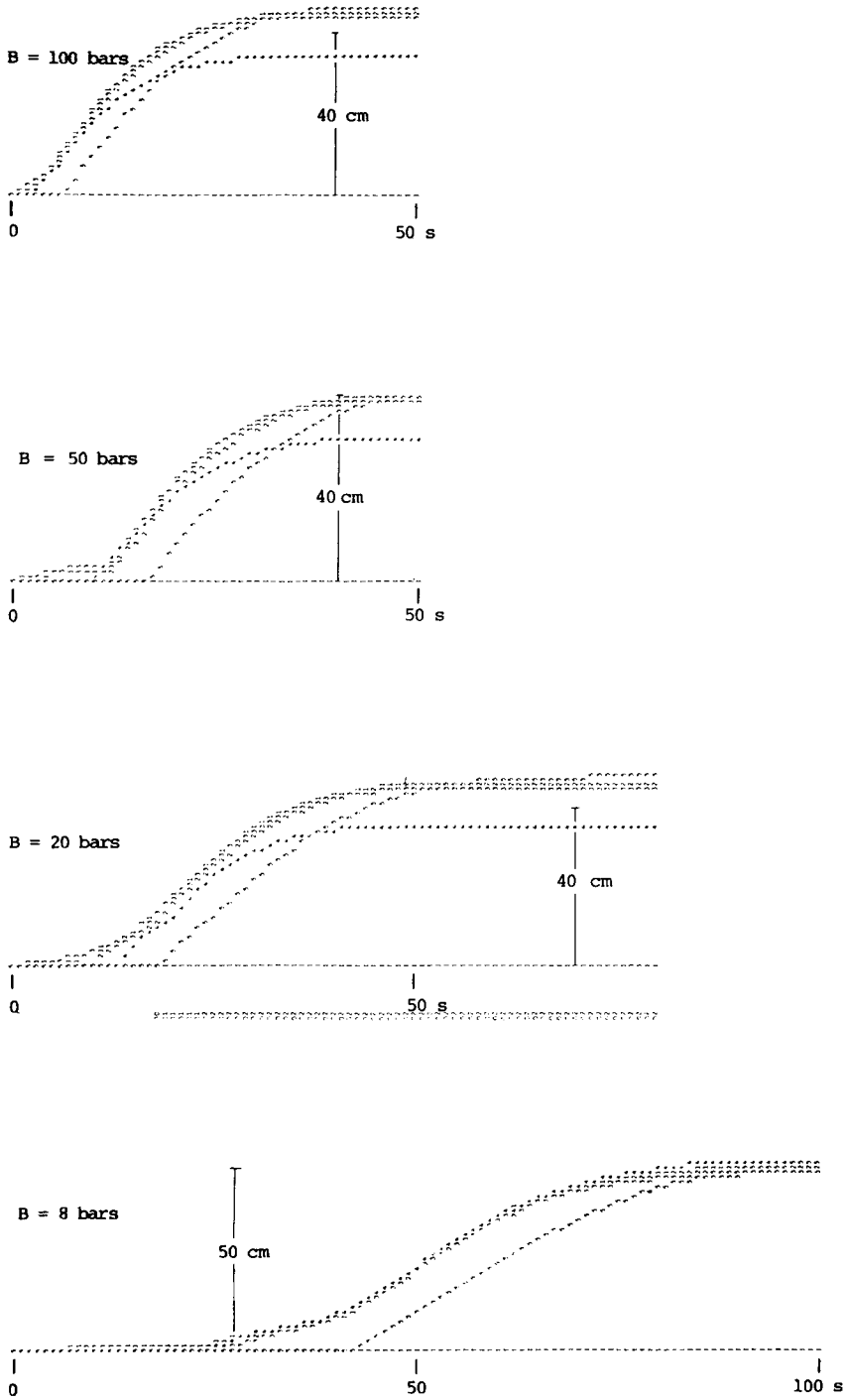

Figure 11(b)

Case C

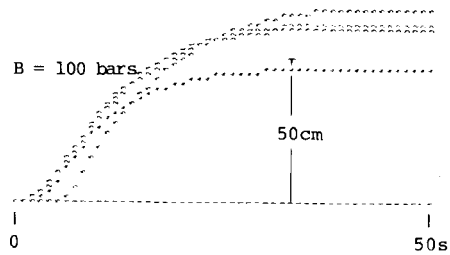

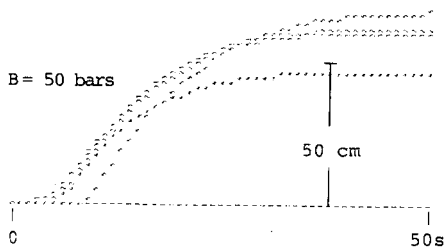

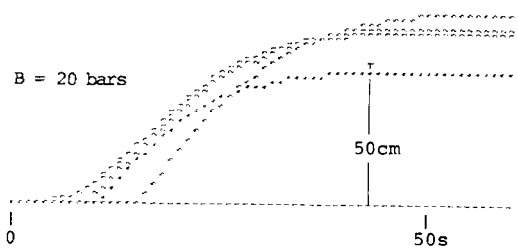

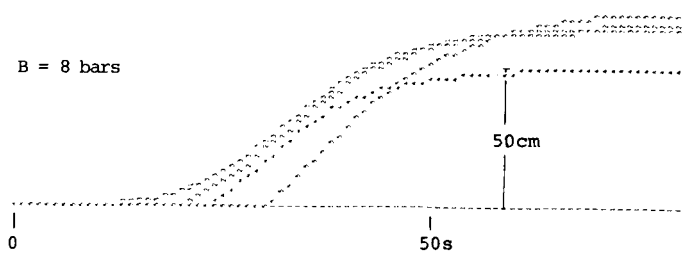

Figure 11 (c)

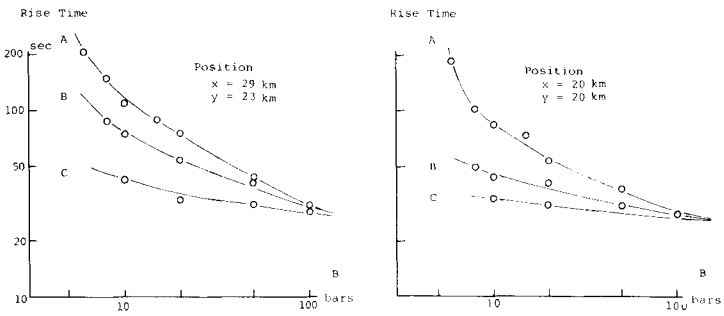

Figure 12. Rise times of the displacement–time functions at two locations, in Cases A, B and C.

It has been shown in Paper I that the normal dynamic rupture process on a heavily non-uniform frictional fault yields stick–slip-like phenomena, which are manifested by episodically rising forms of the displacement time function in several seconds. For a most hetereogeneous fault, Case A in the present case, these minor fluctuations within a short time range are simply masked in the case of larger B-values, whereas for smaller B-values the stick–slip appears more elongated in a longer time range.

Fig. 13 gives the displacement–time function in Case A for $B = 6$ bar. The rise time reaches 200 s at the initiating point of rupture and its vicinity. It is interesting to note that the displacements and stress drops in the nucleus region remain at low levels up to about 130–140 s and then start to develop into larger values. The earlier part might be regarded as a precursory slow movement to the later stage, although the entire displacement time function also shows characteristic features of a slow earthquake. The time which appears to separate the entire function into two parts corresponds approximately to the time by which the slow rupture reaches an edge of the prescribed fault boundaries. if this is true, it seems that propagating energies of the slow moving rupture are blocked by the boundaries and then turned back into the inside of the fault.

4 Discussion

It has been shown in the present paper that the velocity dependence of sliding frictional stress based on the cohesive properties of fault asperities, heterogeneous fault strengths, as well as the initial stress level with respect to the average frictional strength, would play a dominant role in generating slow earthquakes. On the other hand, Yamashita (1980) concluded that a low initial stress combined with low decreating rates in the difference between the initial stress and sliding frictional stress with respect to the distance from the rupture initiating point, and high specific fracture energy will yield slow earthquakes. In the present calculations, we have dealt with the case corresponding to the lowest rate with a constant initial stress, including other possible sources. The fracture energy for creating a new crack surface at the advancing crack tip may be related to the cohesive strength of fault material, and would have some relation with the present case.

Non-elastic properties of fault zone material suggested in several researches might also be able to provide some explanations. For the case of viscous friction on the fault surface, the sliding frictional stress σ_d would be $\sigma_d = \sigma_0 - \eta V/d$, taking into account the constitutive equation $\sigma = \eta\dot{\epsilon}$, where η is the viscosity, d is the thickness of a gouge layer, and $\dot{\epsilon}$ is the strain rate. When σ_0 reaches the level of σ_s, σ_d drops from σ_s in a linear proportion to slip velocity V. If this is tentatively compared with the experimental relation (4) in the present

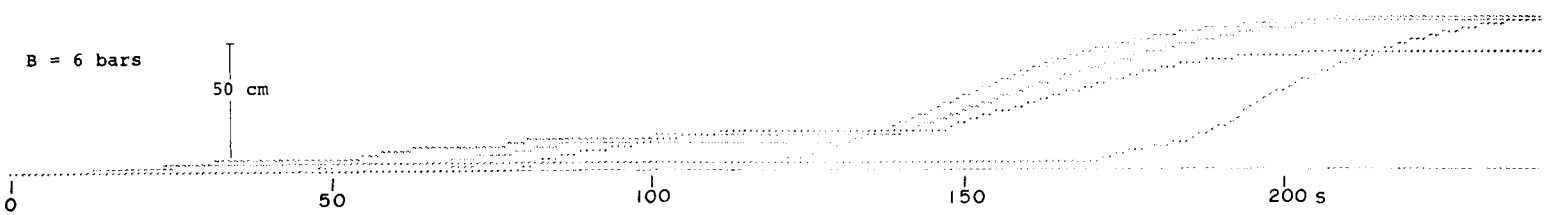

Figure 13. Displacement–time function in Case A for $B = 6$ bar. Different symbols indicate the function at the locations given in Fig. 6. Note that the function suggests stick–slip-like behaviours in this time interval.

case, η/d would correspond to $B \log V/V$, and hence η would be of the order of 10^8 poise for $B = 10$ bar, $V = 2$–10 cm s^{-1} and $d = 10$ m. This does not seem to be an acceptable value, although this oversimplified assumption does not necessarily rule out the possibility of non-elastic models.

It has been reported in the literature (Ando 1975) that the duration time of faulting for earthquakes recurrent on the same fault plane is not always constant as manifested in the 1854 Ansei II and 1946 Nankaido earthquakes. If this is true, a single fault could generate a slow earthquake in one period and a normal brittle earthquake in another. This feature might be explained by a temporal difference in the state of fault zone material such as partial melting and adherence. The present results may provide another interpretation; faulting motion during a large-scale earthquake would break the contact of asperities on the fault surface, and consequently the cohesive strength of ploughing asperities and heterogeneous frictional strength would become considerably different at the time of a succeeding earthquake when the tectonic shear stress again reaches the level of the lowest frictional strength.

The present numerical results show that unusually slow ruptures with small displacements and stress drops could grow up in a limited nucleus region on a strongly heterogeneous fault with smaller B-values and high average frictional strength with respect to the initial stress. The slow rupture develops into subsequent larger slip movements, indicating a stick–slip-like phenomena, after the time it reaches the fault edges. These features appear consistent with those for laboratory friction experiments and their simulation including preseismic stable slip and transient unstable slip motion (Dieterich 1979). The time duration in the present study had to be limited to within 4 min, but if dynamic or quasi-static solutions could be extended to much longer times, the natures of preseismic slip and its triggering mechanism for a normal earthquake would be more explicitly elucidated.

5 Conclusions

We have investigated a possible mechanism to generate slow earthquakes through the dynamical rupture process on a quasi-three-dimensional fault with heterogeneous frictional strength, taking into consideration experimental friction laws for the cohesive properties of indentation and ploughing fault asperities. The effective factors to yield slow earthquakes we have found here are the dependence of sliding frictional stress on slip velocity based on the cohesive properties, which is indicated by a coefficient B, spatially heterogeneous distribution of static and sliding frictional stresses, σ_s and σ_d, and the difference in the level between the applied shear stress σ_0 and the average frictional strength σ_s. The main results from the present numerical calculations are as follows:

(1) For smaller B-values the sliding frictional stress and hence the initial stress does not drop very rapidly with time. For a fixed value of σ_s, the rupture velocity remarkably decreases with decreasing B-values, which give appreciable deceleration effects.

(2) For a fixed B-value, the rupture velocity decreases as the difference in the stress level $\sigma_s - \sigma_0$ becomes larger.

(3) For smaller B-values and larger difference in the stress level $\sigma_s - \sigma_0$, the growth of rupture is extremely slow in a region with a dimension of about six to ten times the initial rupture length. The rupture velocity then slowly increases and reaches a terminal velocity dependent of the B and $\sigma_s - \sigma_0$ values.

(4) Heterogeneous distribution of static and sliding frictional stresses has also noticeable deceleration effects on rupture propagation. As high strength inclusion increases, the rupture velocity goes down to extremely low values in a nucleus region.

(5) The displacement–time function becomes greatly elongated with decreasing B- and increasing $\sigma_s - \sigma_0$ values and increasing heterogeneities. For a strongly heterogeneous fault, the function shows a stick–slip-like phenomena in an extended time interval.

Acknowledgments

I wish to thank Drs Takashi Miyatake, Michio Otsuka and Teruo Yamashita for several discussions and comments on this study. My thanks are also due Professor Tokuji Utsu for citing his results in advance of publication, and Professor Christopher Scholz and Dr James H. Dieterich for generous permission to reproduce their results. Professor Frank F. Evison kindly read through the manuscript and provided suggestions for its improvements.

The numerical computations were made at the Data Processing Center, Kyoto University.

References

Ando, M., 1975. Source mechanisms and tectonic significance of historical earthquakes along the Nankai trough, Japan, *Tectonophys.*, **27**, 119–140.

Andrews, D. J., 1976. Rupture velocity of plane strain shear cracks, *J. geophys. Res.*, **81**, 5679–5687.

Bowden, F. P. & Tabor, D., 1964. *The Friction and Lubrication of Solids, Vol. 2*, Clarendon, London.

Bufe, C. G., Bakun, W. H. & Tocher, D., 1973. Geophysical studies in the San Andreas fault zone at the Stone Canyon Observatory, California, Proceedings of a Conference on the tectonic problems of the San Andreas fault system, eds Kovach, R. L. & Nur, A., *Publ. Geol. Sci. Stanford Univ.*, **XIII**, 86–93.

Burridge, R., 1973. Admissible speeds for plane-strain self-similar cracks with friction but lacking cohesion, *Geophys. J. R. astr. Soc.*, **35**, 439–455.

Dieterich, J. H., 1978. Time-dependent friction and the mechanics of stick–slip, *Pageoph.*, **116**, 790–806.

Dieterich, J. H., 1979. Modeling of rock friction, 1. Experimental results and constitutive equations; 2. Simulation of preseismic slip, *J. geophys. Res.*, **84**, 2161–2175.

Dziewonski, A. & Gilbert, F., 1974. Temporal variations of the seismic moment tensor and the evidence of precursive compression for two deep earthquakes, *Nature*, **247**, 185–188.

Fujii, Y., 1978. Phases and characteristics of seismic crustal movement with special references to Japanese earthquakes, *Bull. Geogr. Surv. Inst., Japan*, **XXIII**, 7–81.

Fukao, Y., 1979. Tsunami earthquakes and subduction process near deep-sea trenches, *J. geophys. Res.*, **84**, 2303–2314.

Fukao, Y. & Furumoto, M., 1975. Mechanism of large earthquakes along the eastern margin of the Japan Sea, *Tectonophys.*, **26**, 247–266.

Geller, R. J. & Shimazaki, K., 1978. The June 10, 1975 Kurile Islands tsunami earthquake, *Proc. Conf. III*, Fault mechanics and its relation to earthquake prediction, pp. 213–226, ed. USGS.

Ida, Y., 1974. Slow-moving deformation pulses along tectonic faults, *Phys. Earth planet. Int.*, **9**, 328–337.

Kanamori, H., 1972. Mechanism of tsunami earthquakes, *Phys. Earth planet. Int.*, **6**, 346–357.

Kanamori, H. & J. J. Cipar, 1974. Focal processes of the great Chilean earthquake May 22, 1960, *Phys. Earth planet. Int.*, **9**, 128–136.

Kanamori, H. & Stewart, G. S., 1979. A slow earthquake, *Phys. Earth planet. Int.*, **18**, 167–175.

Kasahara, M. & Sasatani, T., 1979. Strain seismograms from a large intermediate-depth earthquake of Dec. 6, 1978 near the Kunashiri strait, *Progr. Abstr., seism. Soc., Japan*, **1**, A32.

King, C. Y., Nason, R. D. & Tocher, D., 1973. Kinematics of fault creep, *Phil. Trans. R. Soc.*, **274A**, 355–360.

Major, M. W. & Tocher, D., 1971. Deformation without earthquakes, the central Aleutians, *Abstr. geol. Soc. Am.*, **3**, 154.

Mikumo, T. & Miyatake, T., 1978. Dynamical rupture process on a three-dimensional fault with non-uniform frictions, and near-field seismic waves, *Geophys. J. R. astr. Soc.*, **54**, 417–438.

Mikumo, T. & Miyatake, T., 1979. Earthquake sequences on a frictional fault model with non-uniform strengths and relaxation times, *Geophys. J. R. astr. Soc.*, **59**, 497–522.

Miyatake, T., 1980. Numerical simulations of earthquake source process by a three-dimensional crack model, *J. Phys. Earth*, **29**, submitted.

Nagamune, T., 1977. Time characteristics of crustal deformation of the Yunnan earthquake of May 29, 1976, as inferred from tilt recording, *J. Phys. Earth*, **25**, 209–218.

Nason, R. D., 1971. Measurements and theory of fault creep slippage in central California, *Bull. R. Soc. N.Z.*, **9**, 181–187.

Nason, R. D. & Weertman, J., 1973. A dislocation theory and analysis of fault creep events, *J. geophys. Res.*, **78**, 7745–7751.

Pfluke, J. H., 1978. Slow earthquakes, *Proc. Conf. III*, Fault mechanics and its relation to earthquake prediction, pp. 447–468, ed. USGS.

Sacks, I. S., Suyehiro, S., Linde, A. T. & Snoke, J. A., 1978. Slow earthquakes and stress redistribution, *Nature*, **275**, 599–602.

Savage, J. C., 1971. A theory of creep waves propagating along a transform fault, *J. geophys. Res.*, **76**, 1954–1966.

Scholz, C. H. & Engelder, J. T., 1976. The role of asperity indentation and ploughing in rock friction – I. Asperity creep and stick–slip, *Int. J. Rock Mech. Min. Sci. Geomech. Abstr.*, **113**, 149–154.

Smith, S. W. & Kind, R., 1972. Regional secular strain fields in southern Nevada, *Tectonophys.*, **14**, 57–69.

Sudo, K., Sasatani, T. & Kasahara, M., 1979. Source process of a large intermediate-depth earthquake of Dec. 6, 1978 near the Kunashiri strait, *Prog. Abstr., seism. Soc., Japan*, **2**, B34.

Tocher, D., 1960. Creep on the San Andreas fault – creep rate and related measurements at Vineyard, California, *Bull. seism. Soc. Am.*, **50**, 396–404.

Weertman, J., 1969. Dislocation motion on an interface with friction that is dependent on sliding velocity, *J. geophys. Res.*, **74**, 6617–6622.

Yamashita, T., 1980. Causes of slow earthquakes and multiple earthquakes, preprint, *J. Phys. Earth*, **28**, 169–190.